

OAK RIDGE
NATIONAL LABORATORY

MANAGED BY UT-BATTELLE
FOR THE DEPARTMENT OF ENERGY



ORNL-27 (4-00)

DOCUMENT AVAILABILITY

Reports produced after January 1, 1996, are generally available free via the U.S. Department of Energy (DOE) Information Bridge.

Web site <http://www.osti.gov/bridge>

Reports produced before January 1, 1996, may be purchased by members of the public from the following source.

National Technical Information Service
5285 Port Royal Road
Springfield, VA 22161
Telephone 703-605-6000 (1-800-553-6847)
TDD 703-487-4639
Fax 703-605-6900
E-mail info@ntis.fedworld.gov
Web site <http://www.ntis.gov/support/ordernowabout.htm>

Reports are available to DOE employees, DOE contractors, Energy Technology Data Exchange (ETDE) representatives, and International Nuclear Information System (INIS) representatives from the following source.

Office of Scientific and Technical Information
P.O. Box 62
Oak Ridge, TN 37831
Telephone 865-576-8401
Fax 865-576-5728
E-mail reports@adonis.osti.gov
Web site <http://www.osti.gov/contact.html>

This report was prepared as an account of work sponsored by an agency of the United States Government. Neither the United States Government nor any agency thereof, nor any of their employees, makes any warranty, express or implied, or assumes any legal liability or responsibility for the accuracy, completeness, or usefulness of any information, apparatus, product, or process disclosed, or represents that its use would not infringe privately owned rights. Reference herein to any specific commercial product, process, or service by trade name, trademark, manufacturer, or otherwise, does not necessarily constitute or imply its endorsement, recommendation, or favoring by the United States Government or any agency thereof. The views and opinions of authors expressed herein do not necessarily state or reflect those of the United States Government or any agency thereof.

Results from ORNL Characterization of Nominal 350 μm LEUCO Kernels from the BWXT G73D-20-69302 Composite

A. K. Kercher and J.D. Hunn, Oak Ridge National Laboratory

This document is a compilation of characterization data obtained on the nominal 350 μm low enrichment uranium oxide/uranium carbide kernels (LEUCO) produced by BWXT for the Advanced Gas Reactor Fuel Development and Qualification Program. A 4502 g composite of LEUCO kernels was produced at BWXT by combining kernels from 8 forming runs sintered in 6 separate lots. 2150 grams were shipped to ORNL. ORNL has performed size, shape, density, and microstructural analysis on riffled samples from the kernel composite.

Table of Contents

1	<i>Summary of results:</i>	3
2	<i>Size and shape measurement: (Hunn, Kercher, Price)</i>	5
2.1	<i>Description of method</i>	5
2.2	<i>Size and aspect ratios</i>	5
3	<i>Optical and electron microscopy of kernel surfaces: (Hunn, Menchhofer, Kercher, Dunbar)</i>	8
3.1	<i>Type 1 kernels (shiny & smooth)</i>	9
3.2	<i>Type 2 kernels (dull & smooth)</i>	11
3.3	<i>Type 3 kernels (lumpy)</i>	12
3.4	<i>Type 4 kernels (dull with shiny faceted crystals)</i>	14
4	<i>Microscopy analysis of kernel polished cross-sections: (Hunn, Menchhofer, Kercher, Dunbar)</i>	16
5	<i>Density measurement: (Hunn, Nunn)</i>	18
6	<i>Appendix: RC_{max}, an alternative shape metric</i>	20
7	<i>References</i>	25

1 Summary of results:

Measurements were made using optical microscopy to determine the size and shape of the kernels. Hg porosimetry was performed to measure density. The results are summarized in Table 1-1. Values in the table are for the composite and are calculated at 95% confidence from the measured values of a random riffled sample. The LEUCO kernel composite met all the specifications in Table 1-1 and demonstrated measurably improved characteristics relative to NUCO kernels from the 69300 composite.¹

Table 1-1: Summary of ORNL reported values versus kernel specification.

Kernel Property	Kernel Specification		Measured Values	
	Average (95% conf)	Critical Limit (95% conf.)	Average (95% conf. range)	Critical Limit (95% conf.)
Mean Diameter (μm)	350 \pm 20	<1% <300 and <1% >400	349.4 – 350.0	<1% <327.2 and <1% >372.2
Aspect Ratio ($D_{\text{max}}/D_{\text{min}}$)	NA	<10% \geq 1.05	NA	<2.09% \geq 1.05 <10% \geq 1.033
Envelope Density (g/cc)	>10.5	NA	10.91 – 10.94	NA

Table 1-2: Summary of BWXT reported values versus kernel specification.

Kernel Property	Kernel Specification		Measured Values	
	Average (95% conf)	Critical Limit (95% conf.)	Average (95% conf. range or lower limit)	Critical Limit (95% conf.)
Mean Diameter (μm)	350 \pm 20	<1% <300 and <1% >400	347.1 – 351.9	<1% <323.3 and <1% >372.4
Aspect Ratio ($D_{\text{max}}/D_{\text{min}}$)	NA	<10% \geq 1.05	NA	<9.1% \geq 1.05 --
Envelope Density (g/cc)	>10.5	NA	10.64 – 10.68	NA

The BWXT results for measuring the same kernel properties are given in Table 1-2. BWXT characterization methods were significantly different from ORNL methods, which resulted in slight differences in the reported results. BWXT performed manual microscopy measurements for mean diameter (50 particles measured) and aspect ratio (142 particles measured); ORNL used automated image acquisition and analysis (4303 particles measured). Diameter measurements were in good agreement. The narrower confidence interval in the ORNL results is due to the greater number of particles measured. Aspect ratio satisfied the specification with greater margin in the ORNL results, again because of the larger sample size. BWXT used the aspect ratio of perpendicular diameters in a random image plane, where one diameter was a maximum or a

minimum. ORNL used the aspect ratio of the maximum and minimum diameters in a random image plane. ORNL results for envelope density were measurably higher than the BWXT results. This is likely due to the Hg pressure used to define the envelope volume. This is discussed further in section 5.

2 Size and shape measurement: (Hunn, Kercher, Price)

2.1 Description of method

Size and shape were measured by shadow imaging a sample of kernels in a random plane with an optical microscope. Image analysis software was used to find the center of each kernel and identify up to 360 points around the perimeter. The particle boundary was defined using a Fast Fourier Transform (FFT) fit (10 harmonics) for all regions that had points identified (i.e., no extrapolation). Data was extracted as both radius and diameter. The terms “radius” and “diameter” are used loosely. “Radius” means the distance from the Kasa fit center^{2,3} to the FFT boundary edge. “Diameter” means the distance from FFT boundary edge to FFT boundary edge on a line passing through the fit center. Data for each kernel was then reported in terms of the mean radius or diameter, the standard deviation in those values, the minimum and maximum radius and diameter, and the ratio of the maximum over the minimum of those values (aspect ratio). The uncertainty in the mean diameter for a single kernel was about $\pm 0.2 \mu\text{m}$. The error in the diameter aspect ratio of a single kernel was calculated to be less than 0.001. These values for each kernel were then compiled and the average, standard deviation, minimum, and maximum for each value was calculated. In addition to reporting the compiled data for the sample, histograms of the mean kernel radius or diameter and the aspect ratios have also been provided to show how these values were distributed in the analyzed sample.

2.2 Size and aspect ratios

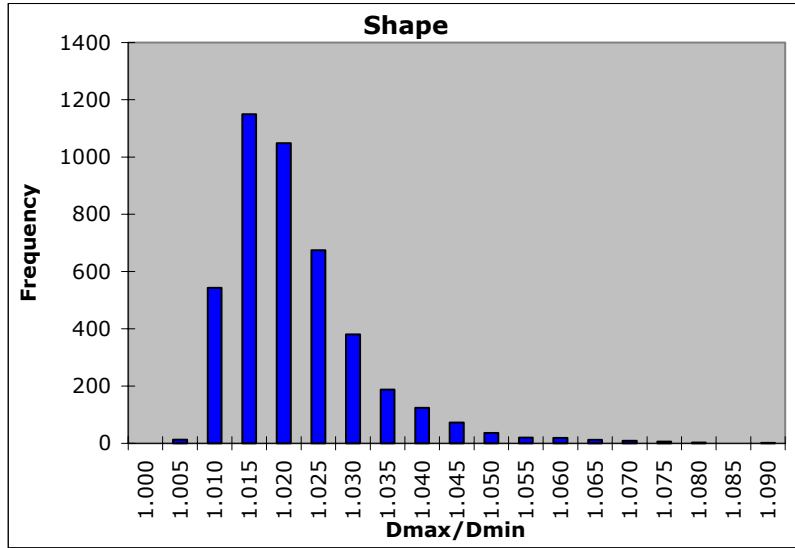
Figure 2-1 shows the summary data for the measured diameter of 4303 kernel shadowgraphs. Figure 2-2 shows the same data reported in terms of the radius. The difference between compiling the measurements in terms of radius versus diameter is that the radius based measurements more accurately report non-symmetric shapes. The diameter measurements dilute the effect of a local deviation in radius by adding the opposite radius (+180 degrees in polar coordinates). The average mean diameter was $349.7 \mu\text{m}$. The mean and standard deviation for radius was one half of the values reported for diameter. However, the radius aspect ratio and diameter aspect ratio (max/min) were quite different, because these values were based on maximum and minimums as opposed to means. Radius aspect ratio, $R_{\text{max}}/R_{\text{min}}$, is a more sensitive way of measuring the deviation from perfectly spherical. The radius aspect ratio measurement showed a higher average and standard deviation (avg. 1.031; $\sigma=0.017$) than the diameter aspect ratio (avg. 1.019; $\sigma=0.0104$).

ORNL has created an alternative shape metric, RC_{max} . Fundamentally different from aspect ratios, RC_{max} quantifies the sharpest feature on the boundary of each kernel shadow. The appendix contains RC_{max} data on LEUCO kernels and direct comparisons with the aspect ratio data.

	Diameter Aspect		St. Dev. In		
	Ratio	Mean Diameter	Diameter	Minimum Diameter	Maximum Diameter
Average	1.019	349.7	1.9	346	353
Standard Deviation	0.0104	9.5	0.99	9.6	9.8
Minimum	1.003	239	0.3	235	242
Maximum	1.125	388	9.8	383	396

Histograms are top-binned

Aspect Ratio (D)	Frequency
1	0
1.005	13
1.01	543
1.015	1150
1.02	1048
1.025	675
1.03	380
1.035	188
1.04	124
1.045	72
1.05	36
1.055	20
1.06	19
1.065	12
1.07	9
1.075	6
1.08	3
1.085	0
1.09	2
>1.09	3



Mean Diameter	Frequency
<280	4
285	1
290	2
295	1
300	1
305	2
310	1
315	2
320	2
325	2
330	18
335	142
340	362
345	661
350	1058
355	949
360	580
365	316
370	130
375	44
380	18
385	4
390	3
>390	0

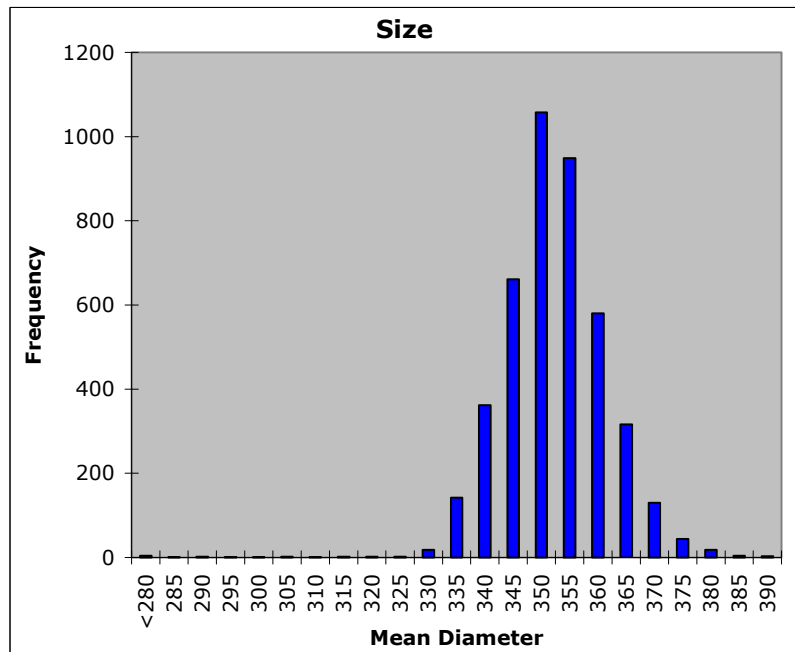
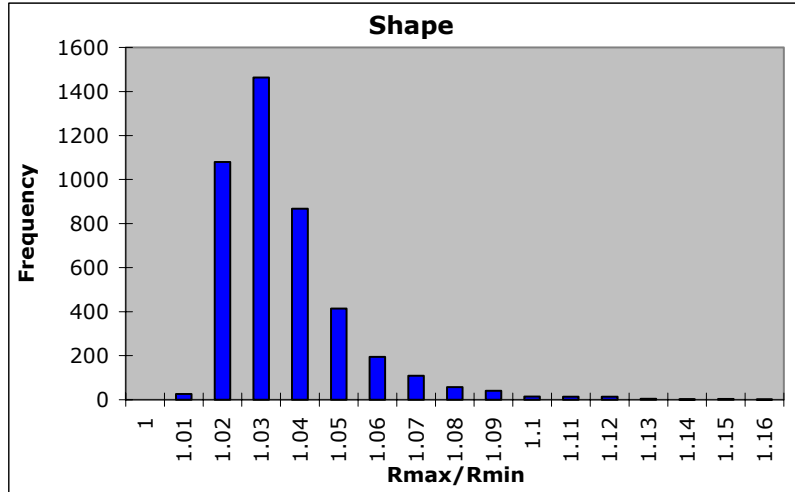


Figure 2-1: Size and shape summary for 4303 LEUCO kernels. Measurements are in μm from edge to edge through best circle fit center.

	Radius Aspect Ratio	Mean Radius	St. Dev. In Radius	Minimum Radius	Maximum Radius
Average	1.031	174.9	1.2	172	178
Standard Deviation	0.017	4.7	0.6	4.9	5.2
Minimum	1.007	119	0.3	115	122
Maximum	1.228	194	6.2	190	201

Histograms are top-binned

Aspect Ratio (R)	Frequency
1	0
1.01	26
1.02	1080
1.03	1463
1.04	867
1.05	414
1.06	195
1.07	108
1.08	57
1.09	40
1.1	14
1.11	13
1.12	13
1.13	4
1.14	2
1.15	3
1.16	1
>1.16	3



Mean Radius	Frequency
<140	4
142	1
144	2
146	0
148	1
150	1
152	1
154	1
156	2
158	1
160	2
162	0
164	7
166	50
168	156
170	313
172	494
174	765
176	876
178	668
180	439
182	274
184	143
186	50
188	32
190	14
192	2
194	4
>194	0

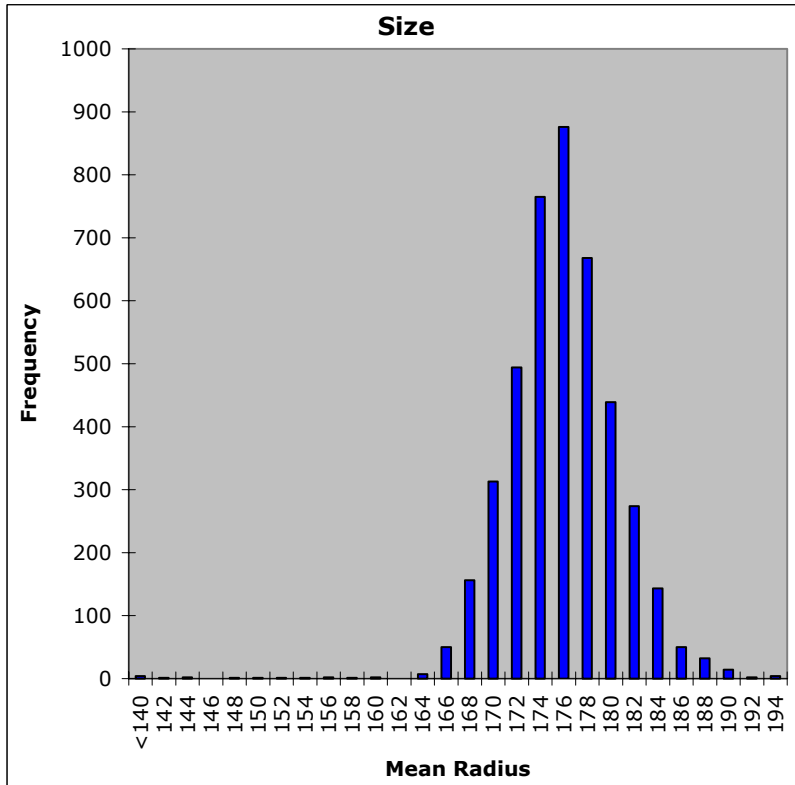


Figure 2-2: Size and shape summary for 4303 LEUCO kernels. Measurements are distance from best circle fit center to edge in μm .

3 Optical and electron microscopy of kernel surfaces: (Hunn, Menchhofer, Kercher, Dunbar)

As shown in Figure 3-1, four different kernel types with different surface appearances were identified in this composite lot of LEUCO kernels: shiny and smooth kernels (Type 1), dull and smooth kernels (Type 2), lumpy kernels (Type 3), and dull kernels with shiny, faceted crystals on portions of the surface (Type 4). Figure 3-2 is a higher magnification image containing the different kernel types. Similar kernel types were observed for a composite lot of BWXT NUCO kernels¹ and a separate single batch of BWXT NUCO kernels.⁴ Because the variety of kernel types was observed for a single batch of NUCO kernels, this microstructural variation suggests a non-uniformity in the forming or heat treatment processes.

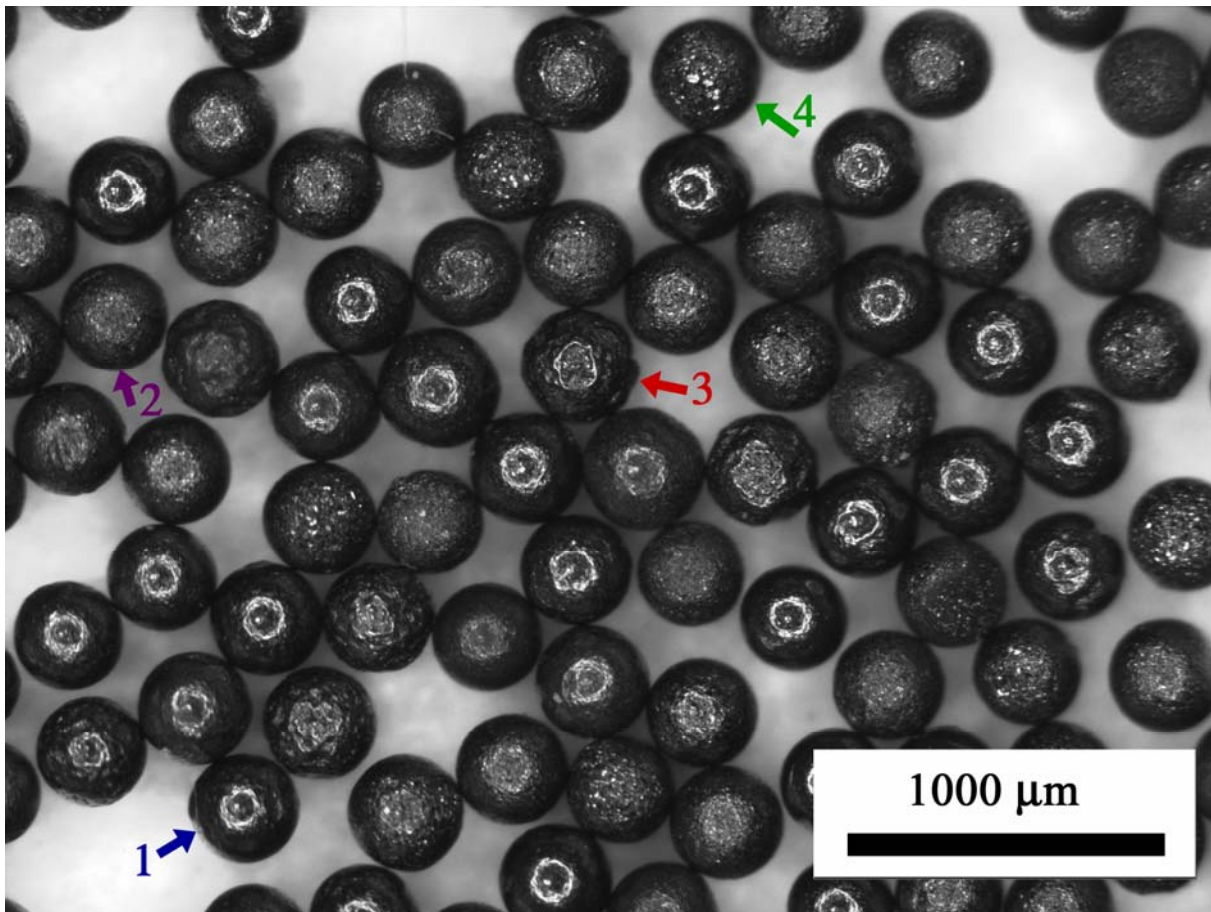


Figure 3-1: This stereoscope image of a typical sample of LEUCO kernels provides examples of the four kernel types: shiny and smooth (Type 1), dull and smooth (Type 2), lumpy (Type 3), and dull with shiny faceted crystals (Type 4). The circular ring observed on the Type 1 kernels is a reflection of the ring light on the stereo microscope.

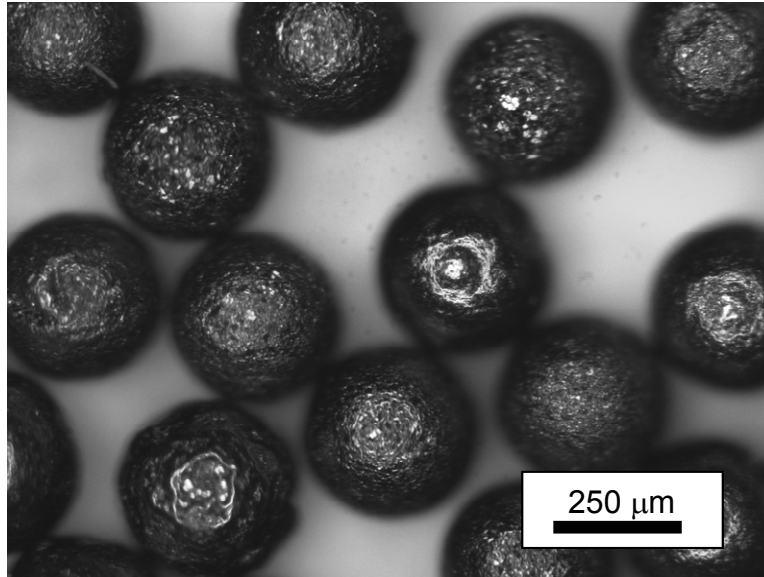


Figure 3-2: High magnification stereoscope image containing the four kernel types.

3.1 *Type 1 kernels (shiny & smooth)*

Approximately 30% of the LEUCO composite lot was comprised of Type 1 kernels (shiny and smooth). Scanning electron microscope (SEM) images of a Type 1 kernel are shown in Figure 3-3 through Figure 3-5. The Type 1 kernel was fairly uniform in appearance with mild shallow pits across most of the surface. The Type 1 kernels often had no gross roughness and seemed to typically have fairly low aspect ratios. Flats and slight elliptical shapes were typical sources of asphericity.

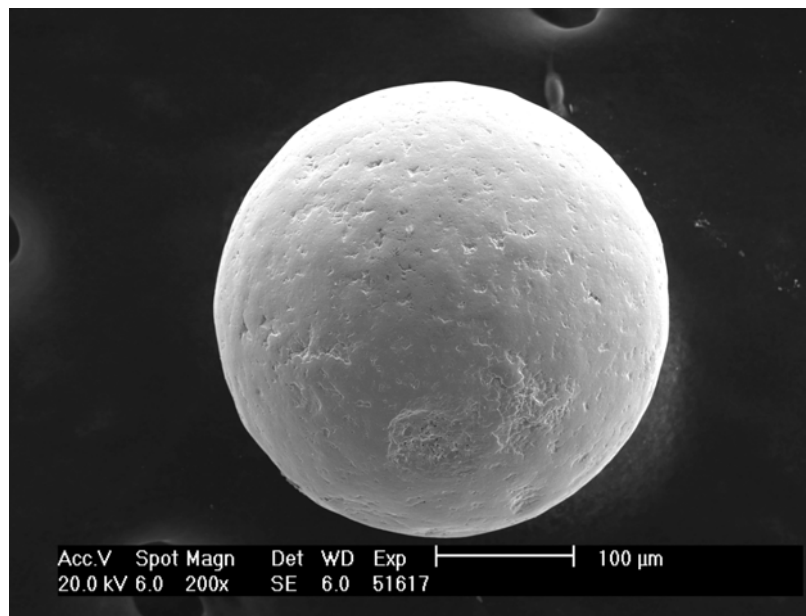


Figure 3-3: Low magnification SEM image of a Type 1 kernel.

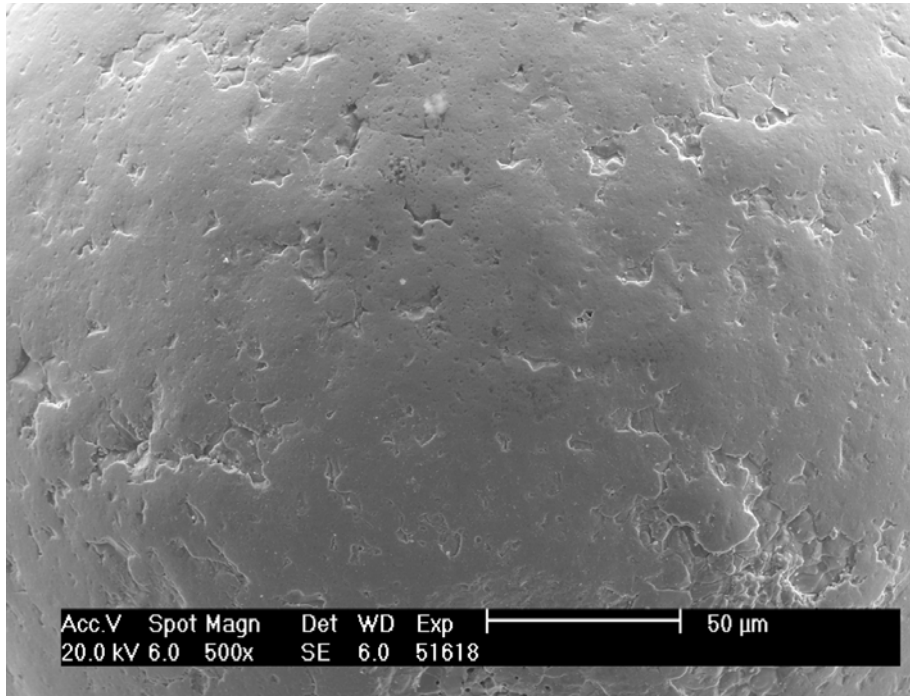


Figure 3-4: SEM image of Type 1 kernel. Note that the majority of the surface is uniform.

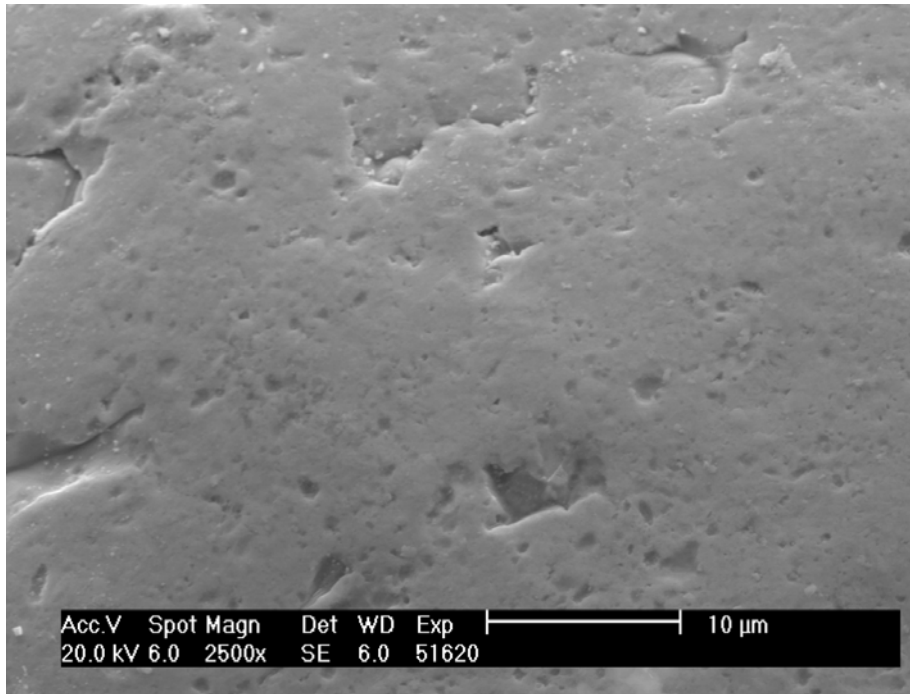


Figure 3-5: High magnification SEM image of Type 1 kernel. Small, shallow pits are prevalent on the surface.

3.2 Type 2 kernels (dull & smooth)

Approximately 40% of the LEUCO composite lot was comprised of Type 2 kernels (dull and smooth). SEM images of two Type 2 kernels are shown in Figure 3-6 through Figure 3-8. The Type 2 kernels were covered with pronounced ~5-10 μm grains. One kernel (#2) had extensive crystallographic steps in its grains; the other kernel had some regions with faint crystallographic steps in its grains. Similar to Type 1 kernels, Type 2 kernels often had no gross roughness and seemed to typically have fairly low aspect ratios. Flats and slight elliptical shapes were typical sources of asphericity.

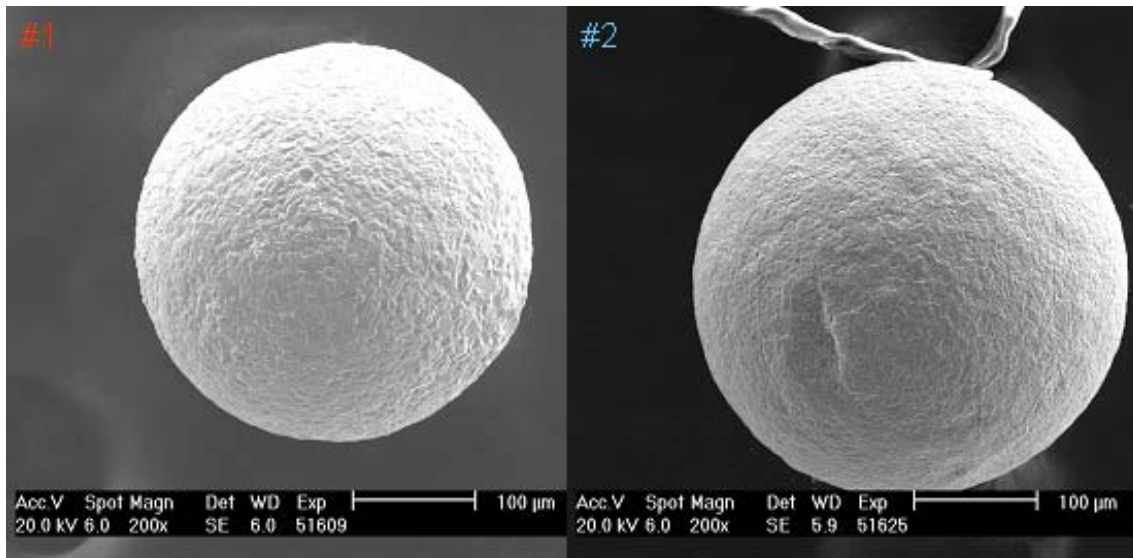


Figure 3-6: Low magnification SEM images of two Type 2 kernels.

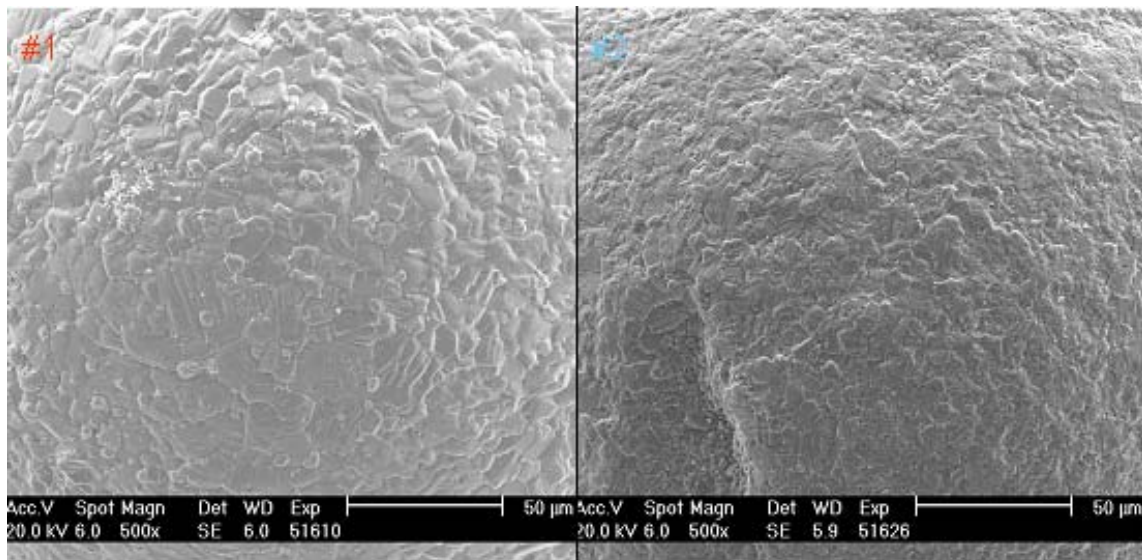


Figure 3-7: SEM images of two Type 2 kernels.

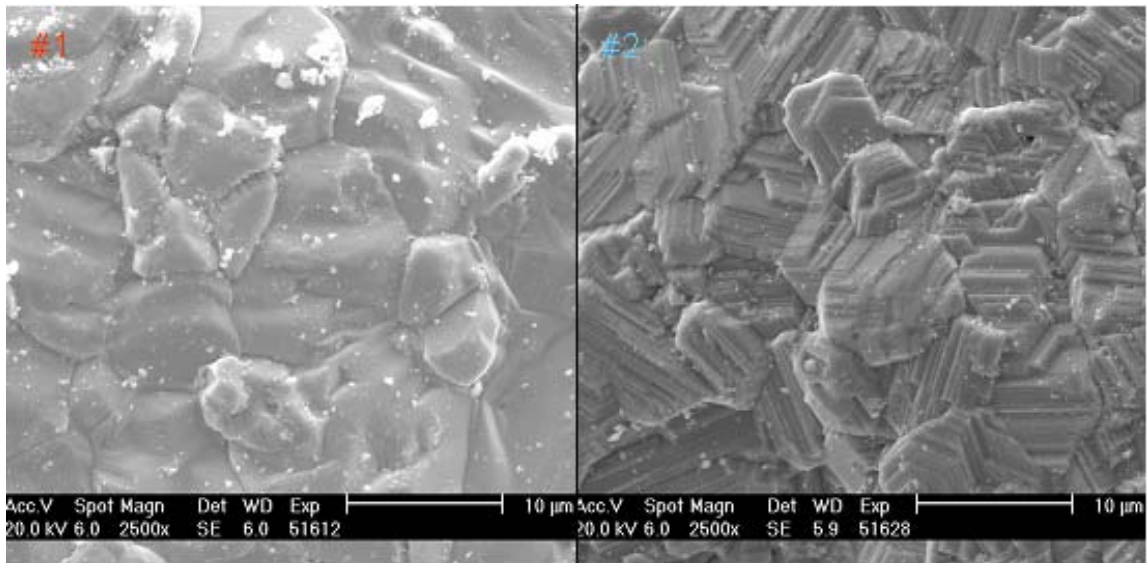


Figure 3-8: High magnification SEM images of Type 2 kernels. The kernel on the right (#2) has pronounced crystallographic steps in its grains.

3.3 Type 3 kernels (lumpy)

Type 3 kernels (lumpy) made up around 15% of the LEUCO composite lot. Type 3 kernels can be considerably misshapen. Some Type 3 kernels were only slightly lumpy and as a result had reasonable aspect ratios (as shown in Figure 3-9). Tabling and other post-production steps may have reduced the fraction of Type 3 kernels. High magnification SEM images of a Type 3 kernel are shown in Figure 3-10 and Figure 3-11. A significant amount of the outer surface had mild shallow pits, similar to the Type 1 kernels. Both Type 3 kernels also had large craters and canyons. The canyons and craters contained large ~5-10 µm grains.

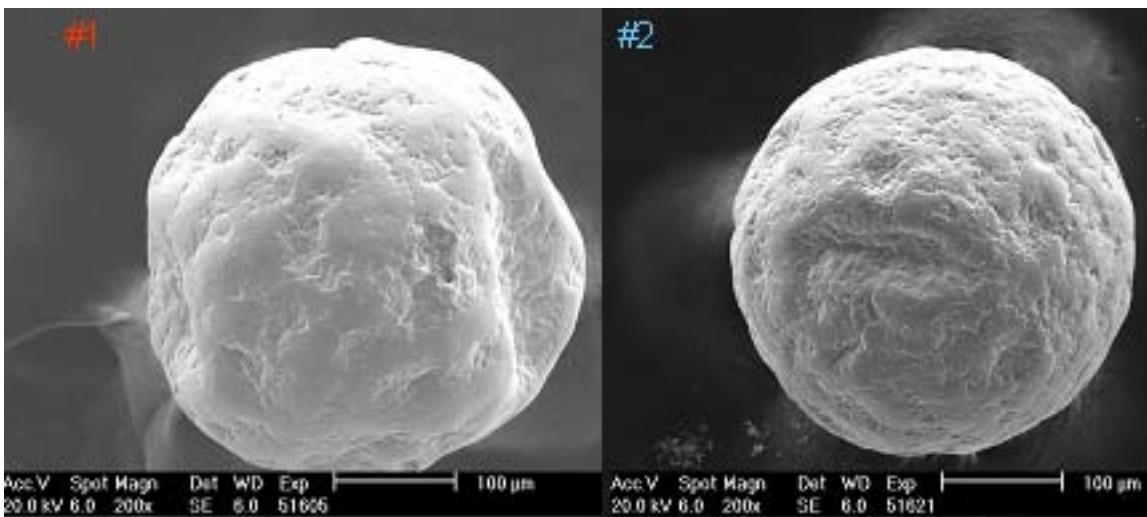


Figure 3-9: Low magnification SEM images of two Type 3 kernels. Kernel #1 is badly misshapen; kernel #2 is approximately spherical despite a large degree of surface topology.

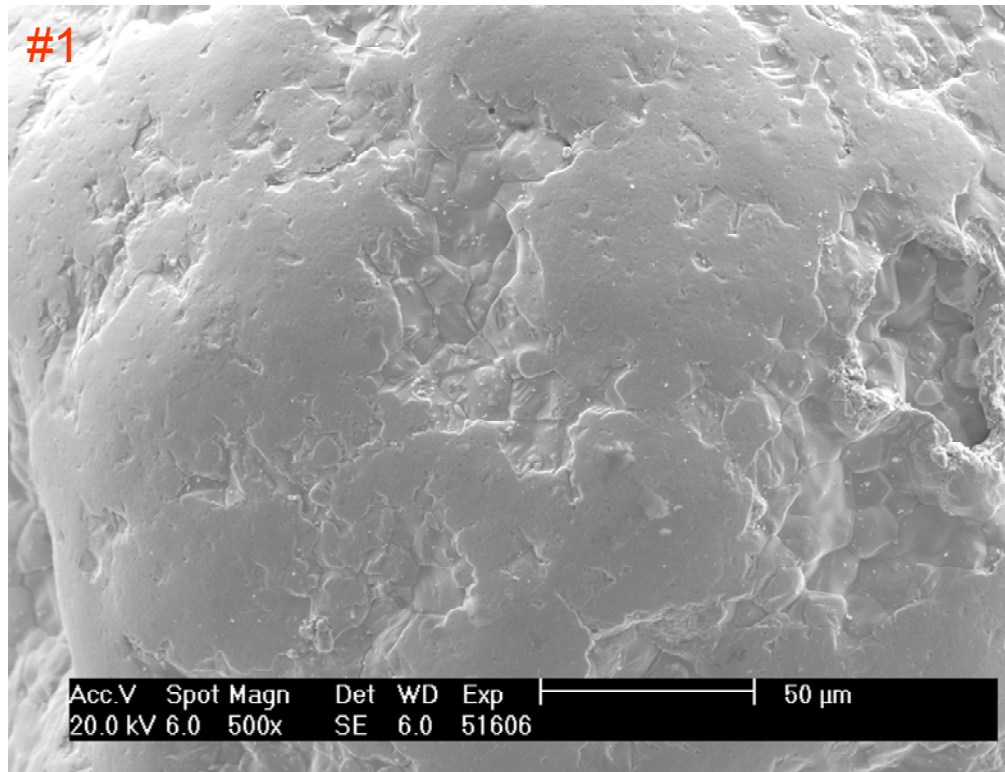


Figure 3-10: SEM image of Type 3 kernel (kernel #1 from Figure 3-9)

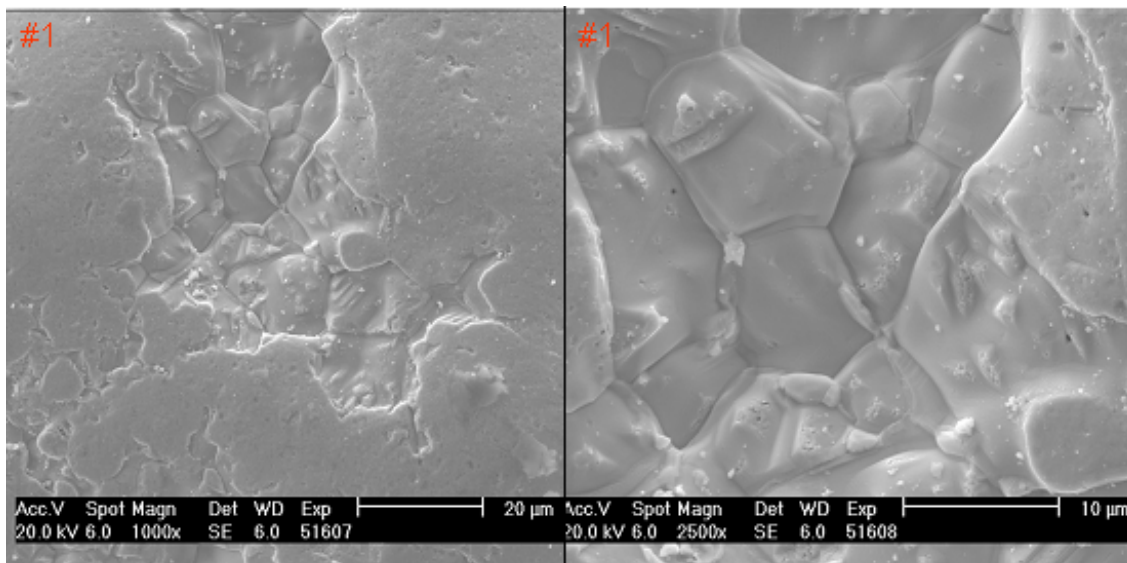


Figure 3-11: High magnification images of a Type 3 kernel (kernel #1 from Figure 3-9). Note the regions with small, shallow pits (similar to Type 1) and the larger craters with clearly visible 5-10 µm grains.

3.4 Type 4 kernels (dull with shiny faceted crystals)

Type 4 kernels were not always identified, because the shiny faceted crystals usually form on only a limited region of the kernel which may be face-down. Type 4 kernels may constitute about 15% of the LEUCO composite lot. Type 4 kernels seemed to vary in aspect ratio more than Type 1 or Type 2 kernels. Figure 3-12 through Figure 3-14 show two Type 4 kernels. The faceted crystals (grains) were ~10-20 μm in diameter. Typical Type 4 kernels exhibited two distinct regions: a region with faceted crystals and a rough surface covered with deep pits. A fluidized bed sintering furnace would not be expected to create kernels with two distinct regions, but BWXT did report problems with kernels sticking inside the fluidized bed furnace.⁵ Type 4 kernels may have been kernels that became stuck inside the furnace during sintering.

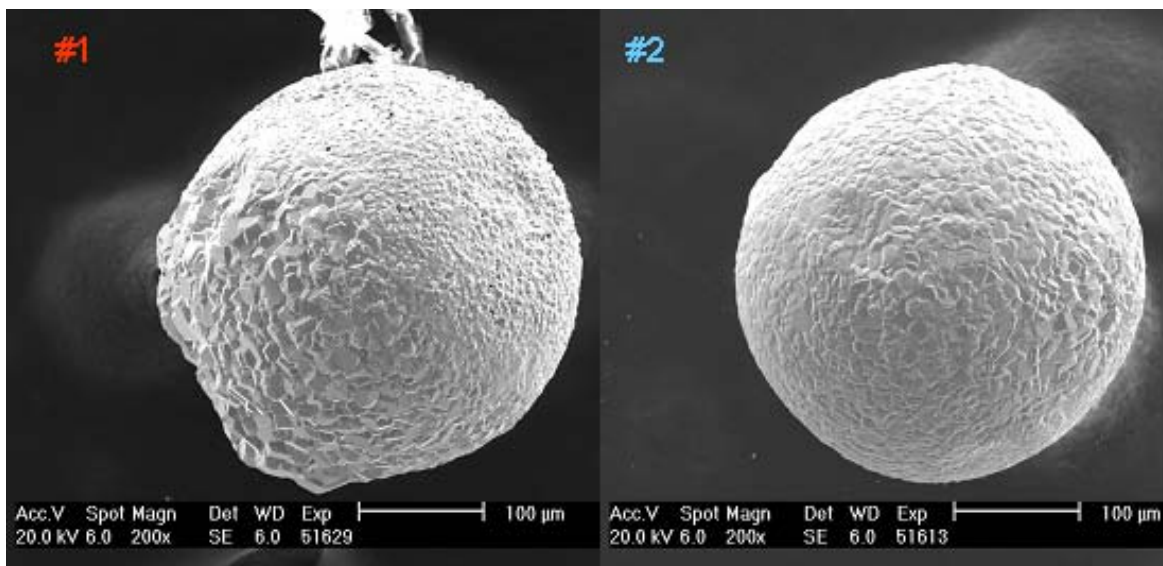


Figure 3-12: Low magnification SEM images of Type 4 kernels. Both kernels have the characteristic large faceted grains. Kernel #1 has more pronounced faceting than kernel #2. Kernel #1 exhibits two regions: a region with large faceted grains and a bumpy porous region.

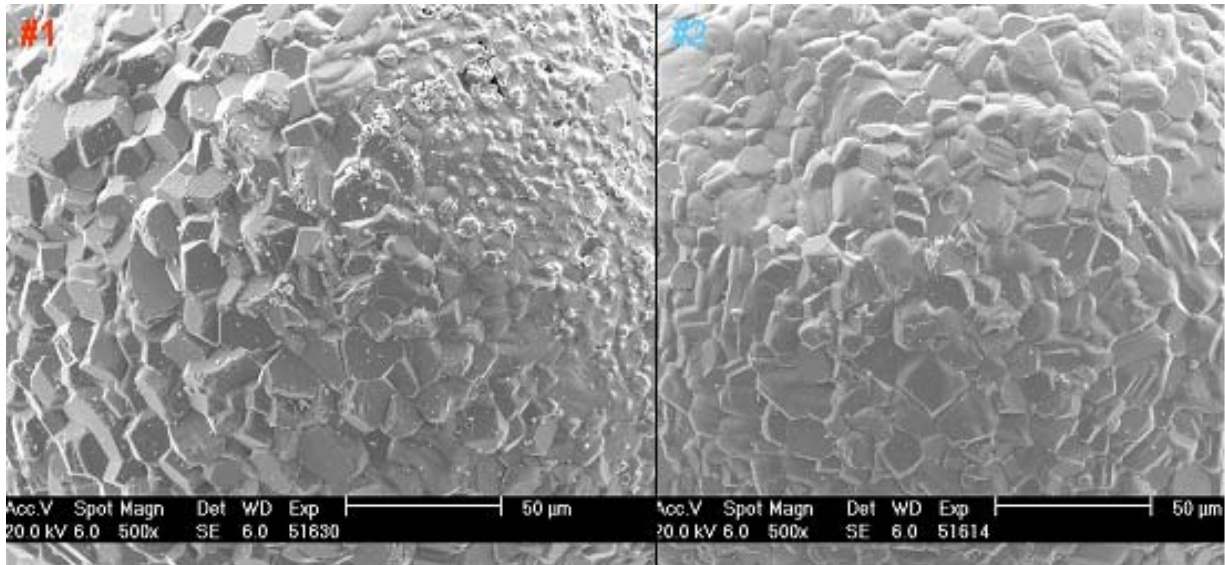


Figure 3-13: SEM images of two Type 4 kernels. Note the deep pits and rough surface of half of kernel #1.

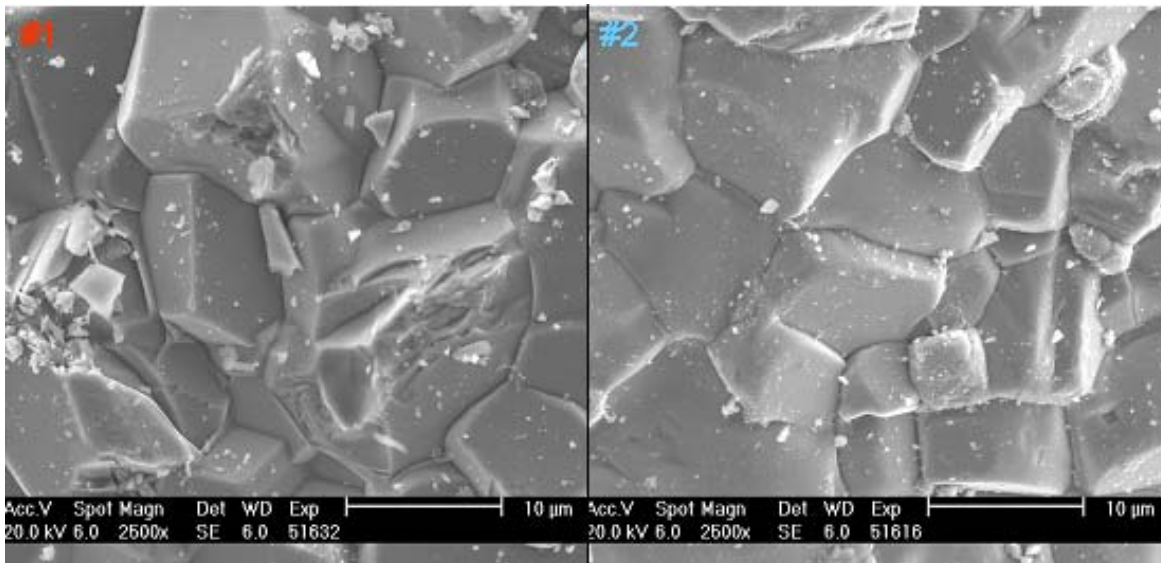


Figure 3-14: High magnification SEM images of two Type 4 kernels. Although both kernels have shiny faceted grains, kernel #2 has rounded edges to many faceted grains (~10-20 µm diameter). Kernel #2 has some similarities to Type 2 kernels (Figure 3-8) and the crater regions on Type 3 kernels (Figure 3-11).

4 Microscopy analysis of kernel polished cross-sections: (Hunn, Menchhofer, Kercher, Dunbar)

Kernels were mounted in conductive epoxy and ground and polished to near the midplane. A contrast variation across the cross section was readily observed both optically (Figure 4-1 and Figure 4-2) and by SEM using back-scattered electrons (BSE). This variation was due to separate oxide and carbide phases as has been discussed in previous reports.^{1, 4} The darker gray areas were oxides and the lighter areas were carbides. An oxide rind was evident on the outside surface of many kernels. As previously discussed,¹ this indicates a carbon depleted zone is formed during heat treatment. The interior of the kernels showed a mixture of oxide and carbide phases.

Pits (black spots) were observed in the LEUCO kernel cross sections. It is difficult to tell how many of the pits were due to material removed during polishing and how much was due to porosity in the kernels. Both were expected. The friability of the kernels was high, which made pullout during polishing likely. Friability also varied considerably. Type 3 kernels tended to show a greater tendency to crumble during cross-sectioning (Figure 4-2). In Figure 4-2, the large hole in the rightmost particle is not a pore but rather is due to a small kernel contained within the full-sized kernel. This phenomena of a small kernel contained within a larger kernel has been described in a previous report.¹ The inner surface of the kernel's hole was observed to be relatively smooth, which further suggested that a distinct smooth object fell out of the kernel cross-section during polishing (Figure 4-3).

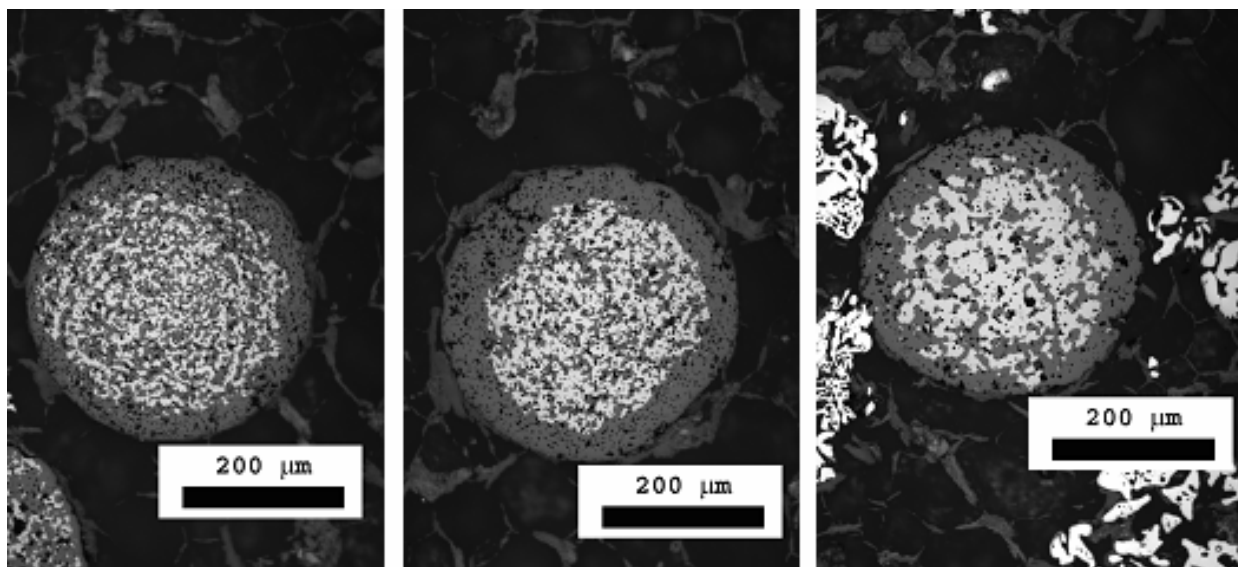


Figure 4-1: Optical microscopy images of polished LEUCO cross-sections with oxide rinds. Note the variability in the internal phase distribution. The apparent porosity may be due to material falling out during polishing.

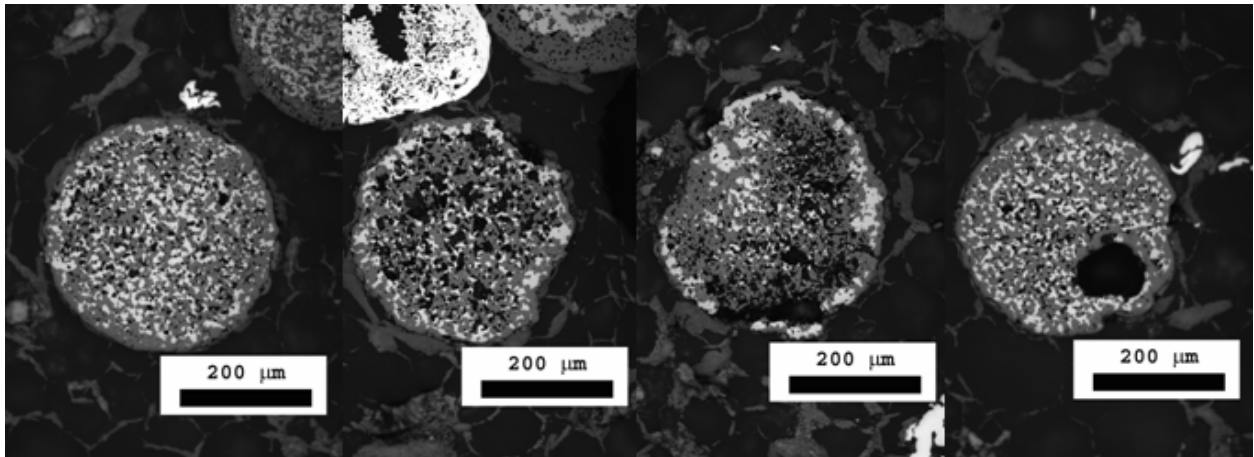


Figure 4-2: Optical microscopy image of polished LEUCO cross-sections without oxide rinds. This microstructure was most often associated with Type 3 kernels. Type 3 kernels also showed more extensive and larger pits, either due to high porosity, higher friability, or both.

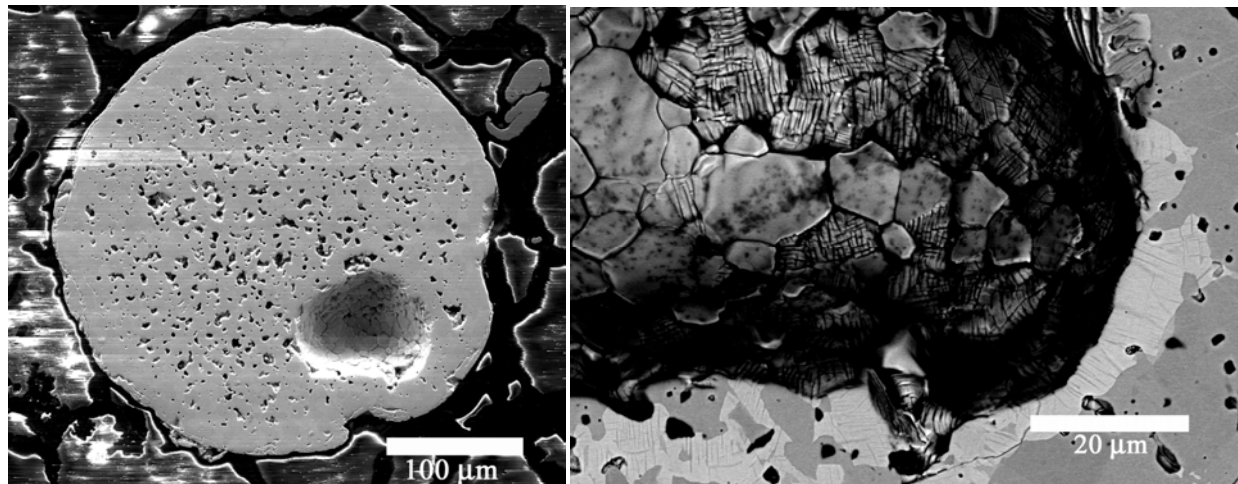


Figure 4-3: SEM micrograph of a kernel shown in Figure 4-2. The hole surfaces are smooth, which indicates that a distinct smooth object fell out of the kernel cross-section. The left image is a secondary electron micrograph. The right image is a backscattered electron micrograph.

5 Density measurement: (Hunn, Nunn)

Using the ASTM D3766 standard terminology, we define four different types of density: the *theoretical density* is based solely on the solid material volume, the *skeletal density* includes the closed pore volume, the *envelope density* includes the open and closed pore volume, and the *bulk density* includes the open and closed pore volume and the interparticle space. The theoretical density of UO_2 is 10.96 g/cc. The theoretical density of UC_2 is 11.28 g/cc. The theoretical density of UC is 13.63 g/cc.

Envelope density was measured with a mercury porosimeter. The mercury pressure used to determine envelope density can have a significant effect on the reported value. The envelope density for this report was measured by weighing a sample and measuring the volume of mercury displaced at 25 psia. When determining the envelope volume, the mercury pressure must be high enough to fill the majority of the interparticle space without filling in a significant amount of the kernel porosity. Packed spheres have interparticle spaces which are partially empty at the initial fill pressure of a mercury porosimeter measurement. These interparticle “pores” become more narrow near the contact points between particles. As applied pressure increases, mercury will be able to fill more of the interparticle porosity near the contact points but it will also start to fill large open pores on the particle surface. Using the Washburn equation for cylindrical pores, mercury can fill pores of approximately 9 μm diameter at 25 psia. Large surface pores or craters in the kernels should be filled during the buffer deposition process, so it is reasonable not to include pores larger than 9 μm in the envelope volume.

Figure 5-1 shows plots of relative intrusion volume versus fill pressure for zirconia and LEUCO kernels. The curve for the non-porous zirconia spheres illustrates how the mercury intrudes into the interparticle volume. In the plot for zirconia in Figure 5-1, 90% of the intrusion volume change occurred below 25 psi. This volume change was due to filling of the interparticle space. The plot in Figure 5-1 for the LEUCO kernels shows more intrusion above 25 psi because there is measurable open porosity being filled in this pressure range. The elbow that occurs around 25 psi indicates where most of the interparticle space has been filled.

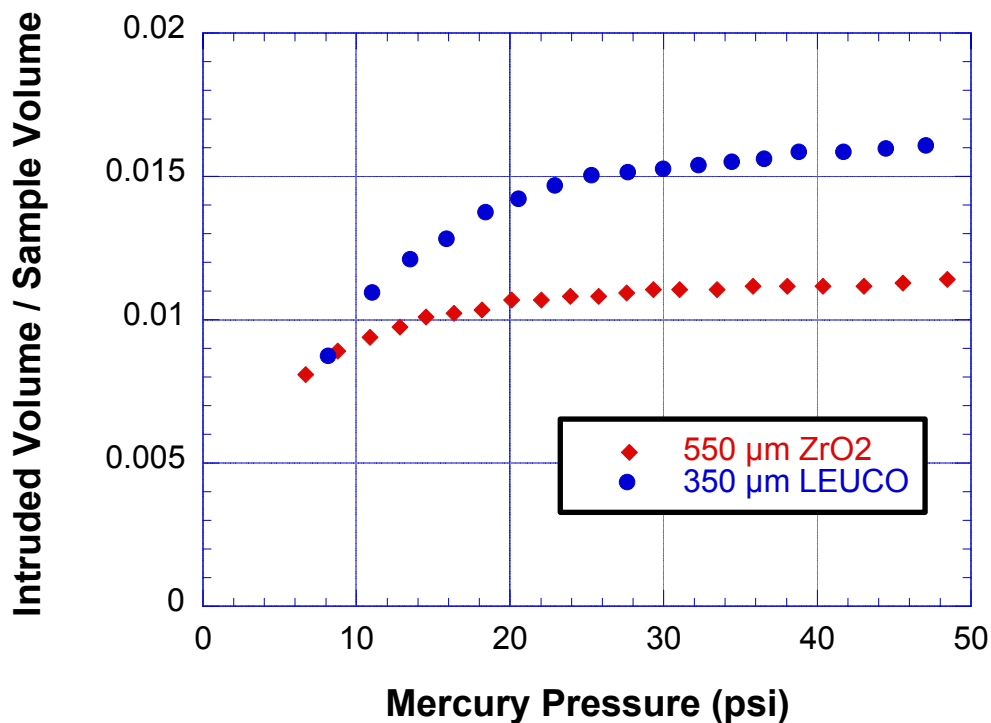


Figure 5-1: Relative intrusion volume versus fill pressure for zirconia and LEUCO kernels.

Several samples were riffled from the LEUCO composite lot. Table 5-1 shows the results of the measurement of envelope density on these samples. The average envelope density was 10.924 g/cc with a standard deviation of 0.015 g/cc. If the interparticle space were not accounted for and the bulk volume at the mercury fill pressure of 5 psi were used instead, the average density for these measurements would be approximately 10.71 g/cc. This value would be more accurately labeled as the bulk density.

Table 5-1: Envelope density by Hg porosimetry

Sample weight (g)	Envelope density (g/cc)
12.582	10.943
12.508	10.925
12.877	10.912
12.645	10.932
12.690	10.906

Average envelope density {g/cc}	10.924
Standard Deviation (sample) {g/cc}	0.015

6 Appendix: RC_{\max} , an alternative shape metric

While kernel shape may ultimately affect particle failure rate in a reactor environment, failure mechanisms based on kernel shape are not well established. Two possible correlations between kernel shape and TRISO fuel failure are: (1) kernel features can propagate through the TRISO coating process to create structural layers with stress concentrators and (2) odd kernel shapes can indicate defective kernels that could cause problems during TRISO fuel manufacture or product irradiation. Large kernel protrusions, flats, and craters have been observed to affect the shape of SiC and pyrocarbon layers in TRISO particles produced at ORNL, but the buffer layer deposition has been observed to seemingly correct for (“smoothen out”) slight aspherical features in the kernel. However, it has been previously reported that lumpy-shaped NUCO kernels are much more friable than smooth-shaped kernels, and kernel shape and internal microstructure are often related.¹

Historically, the diameter aspect ratio of kernels has been used in a tolerance limit specification for quality control purposes, and this could be easily measured with conventional optical microscopy. Kernel aspect ratio has never been strongly correlated to the performance of fuel kernels by experiment or model. Aspect ratio essentially is a descriptor of overall relative dimensions. Except in extreme cases, overall relative dimensions of kernels should not be related to problems in TRISO fuel fabrication or final fuel performance.

An ideal metric for kernel shape would identify *localized kernel features* that could indicate possible problems in TRISO fuel manufacture or product irradiation. A detrimental feature in a kernel may be discernable in a shadow image as a bump, protrusion, or flat. The automated image analysis used at ORNL has allowed for the development of an alternative metric for kernel shape that may have a stronger correlation to processing difficulty and TRISO fuel performance. RC_{\max} , the product of the curvature and the radius at the point of maximum curvature, is a unitless metric that describes the sharpest feature visible on each kernel. The curvature (given in μm^{-1}) was computed in the FFT (fast Fourier transform) domain using 10 harmonics based on the equation:

$$C = \frac{x'y'' - y'x''}{(x'^2 + y'^2)^{3/2}}$$

where x and y represent $x(s)$ and $y(s)$, which are arc-length parameterizations of the 10 harmonic FFT fit boundary points. Figure 6-1 provides a histogram of the RC_{\max} metric for the LEUCO material. Figure 6-2 plots radius and diameter aspect ratio as a function of RC_{\max} and demonstrates only a weak trend. RC_{\max} is a fundamentally different metric than aspect ratio. Figure 6-3 through Figure 6-6 provide kernel images with different RC_{\max} values (radius and diameter aspect ratios given for comparison).

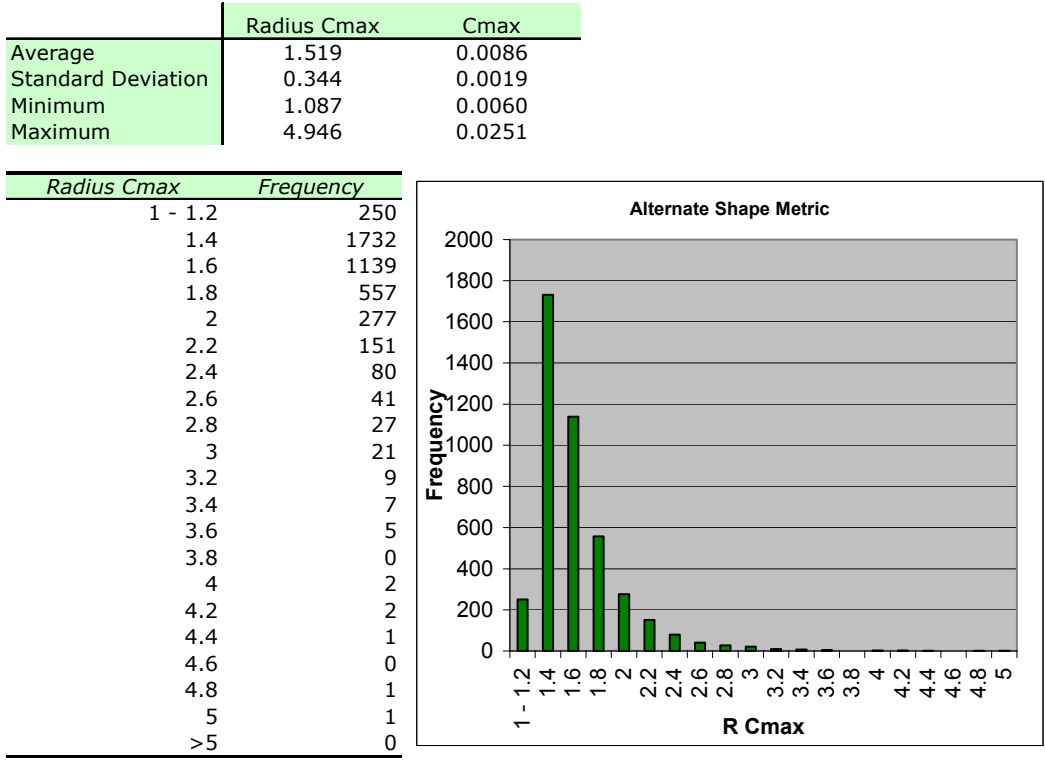


Figure 6-1: Alternative shape metric, RC_{max} . Curvature given in μm^{-1} .

For the 4303 LEUCO kernels, the 99th percentile based on RC_{max} is 2.83. Of the 43 kernels that exceed $RC_{max} = 2.83$, only 21 kernels have a diameter aspect ratio greater than 1.05 (the control limit of the current kernel specification). There are 74 kernels with a diameter aspect ratio greater than 1.05. These figures further demonstrate that kernel specifications based on RC_{max} and diameter aspect ratio can provide drastically different conclusions on kernel quality. If RC_{max} is the appropriate metric for defective kernel shape, a diameter aspect ratio metric could produce a large number of false positives (i.e., designating good kernels as “bad”) and/or false negatives (i.e., not identifying bad kernels).

Although not the focus of this report, RC_{max} has perhaps greater significance when characterizing the shape of TRISO fuel particles. Bumps, flats, and protrusions on TRISO particles should be very representative of the bumps, flats, and protrusions present in underlying SiC and pyrocarbon layers. The sharpness of the corners for bumps, flats, and protrusions would correlate with the stress concentrator severity in underlying layers.

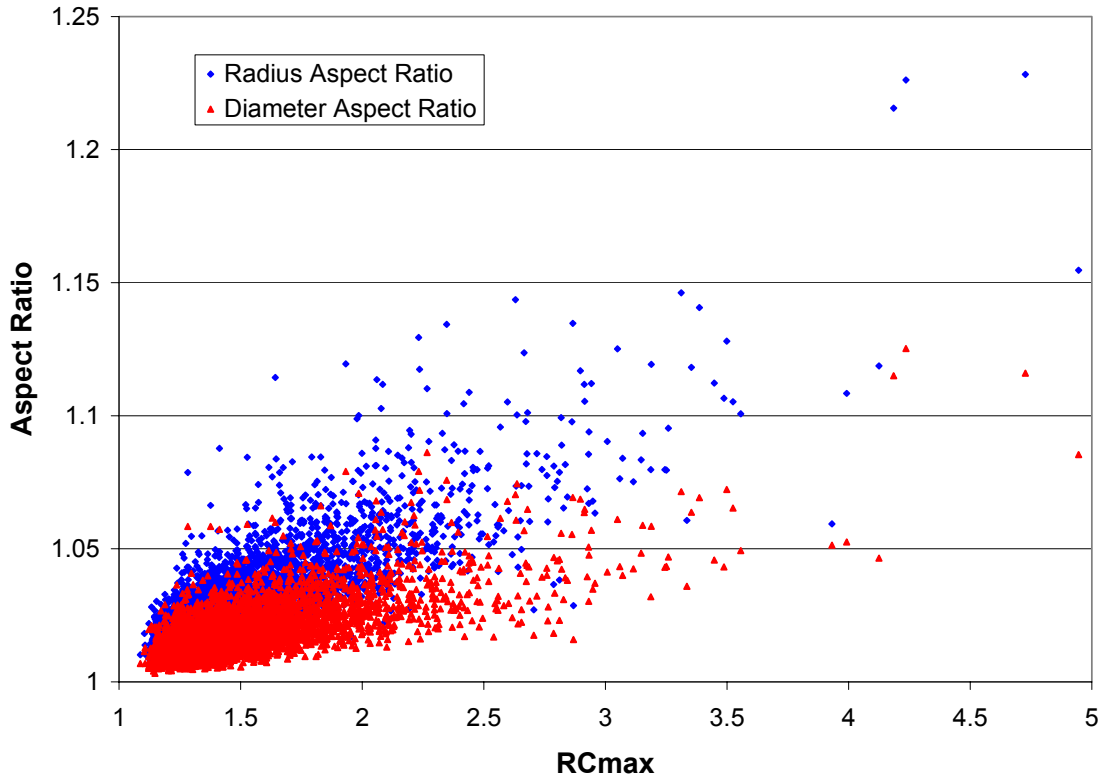


Figure 6-2: Radius and diameter aspect ratio as a function of RC_{max} (4303 kernels).

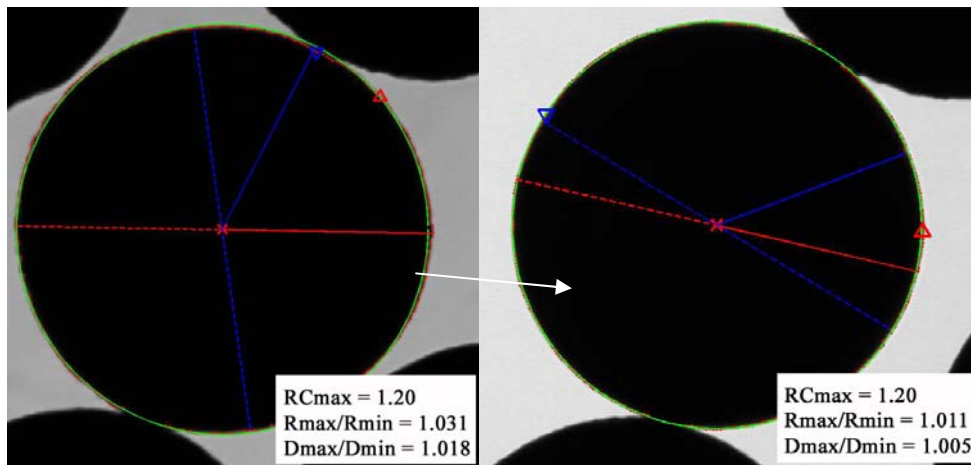


Figure 6-3: Examples of LEUCO kernels with a low RC_{max} (~ 1.2). Aspect ratio data is included for comparison. The blue lines correspond to minimum radius (solid) and diameter (dashed). The red lines correspond to maximum radius and diameter. The red dots are the identified boundary. The green circle is the best fit circle. The red triangle is the boundary location with maximum curvature. The inverted blue triangle is the boundary location with minimum curvature. Particle sizes should not be compared, because images are shown at various magnifications. RC_{max} is less sensitive to a slight elliptical character than aspect ratio.

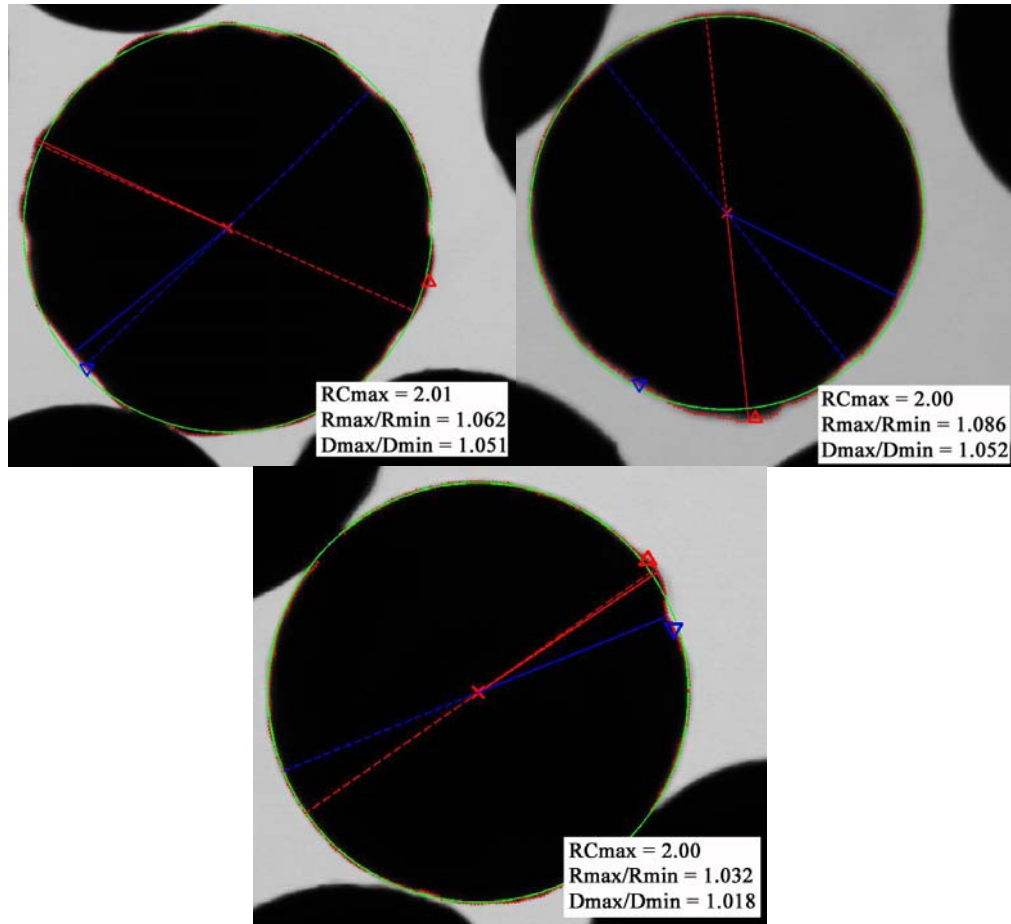


Figure 6-4: LEUCO kernels with RC_{max} approximately equal to 2. Aspect ratio data is given for comparison. Aspect ratios are not consistent metrics for bumps, flats, and chips.

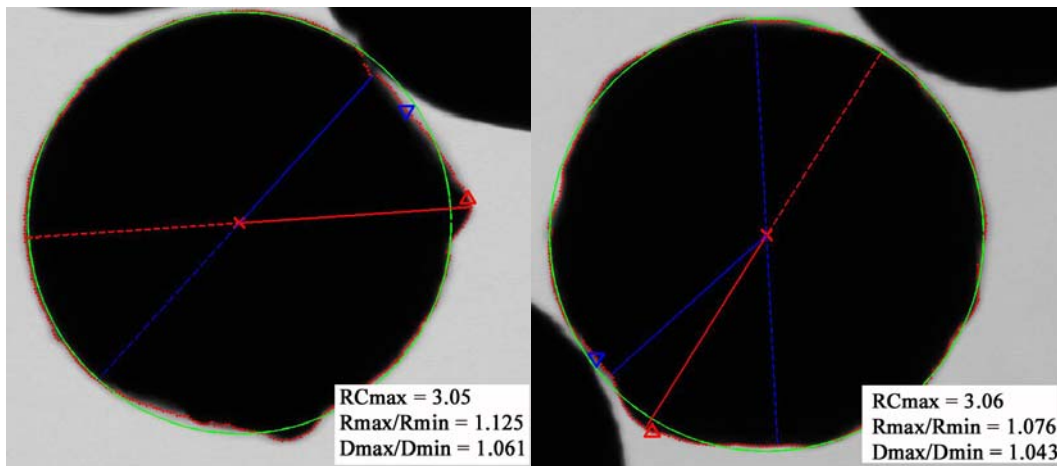


Figure 6-5: LEUCO kernel with an RC_{max} approximately equal to 3. While these defects may be severe enough to affect deposited layer shapes, the diameter aspect ratio of the particle on the right is below the current critical limit specification of 1.05.

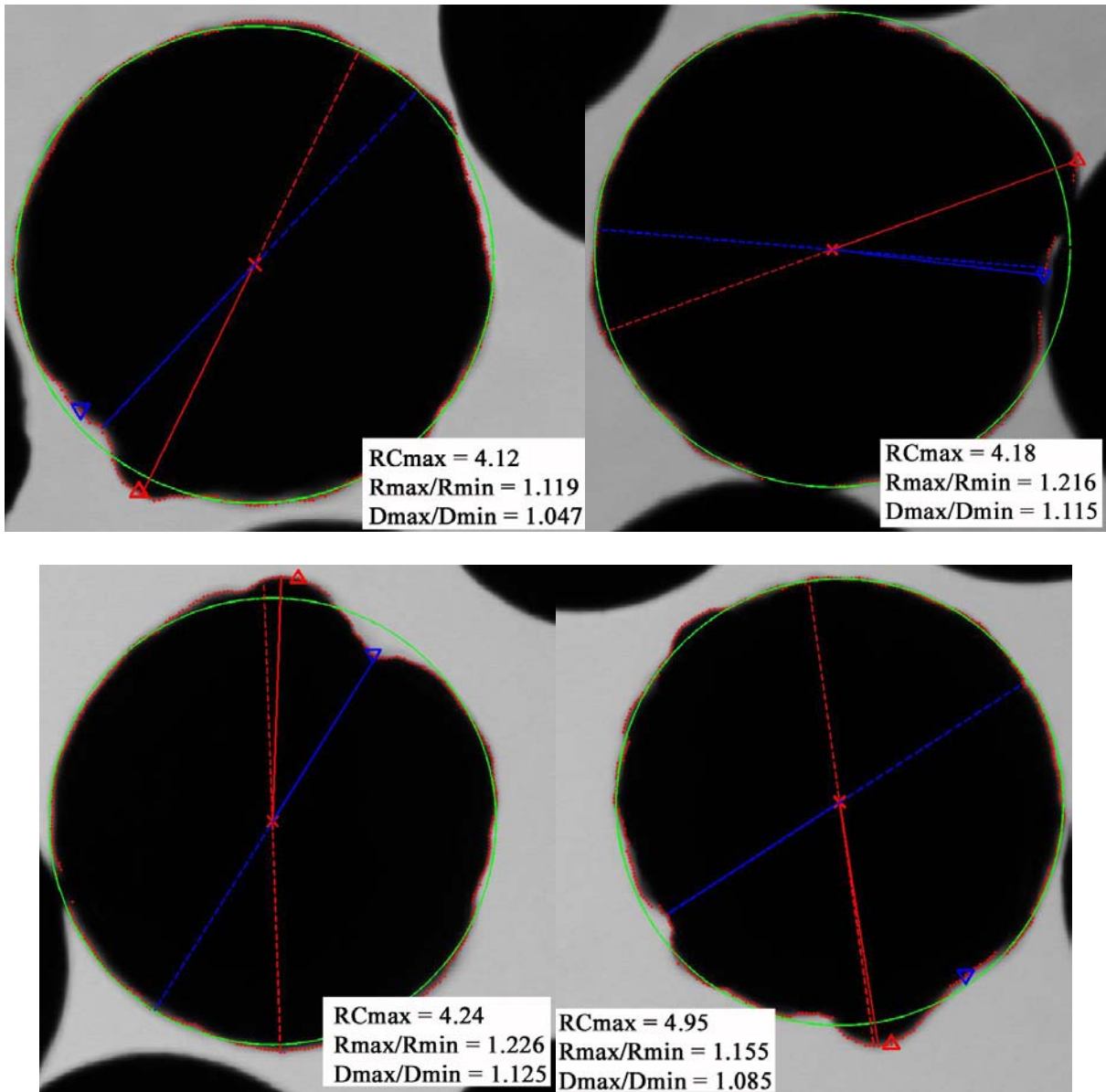





Figure 6-6: LEUCO kernels with RC_{max} approximately equal to 4. Aspect ratios are given for comparison. These kernels all exhibited severe defects. The upper left kernel has a low enough diameter aspect ratio to pass the current critical limit specification of 1.05.

7 References

1. Hunn JD. "Results from ORNL Characterization of Nominal 350 μm NUCO Kernels from the BWXT 69300 composite." Document# ORNL/CF-04/07. Sept 2004.
2. Kasa I. A circle fitting procedure and its error analysis. IEEE Transactions on Instrumentation and Measurement 1976; 25(1): 8-14.
3. Rusu C, Tico M, Kuosmanen E, Delp E. Classical geometrical approach to circle fitting – review and new developments. Journal of Electronic Imaging 2003; 12(1): 179-193.
4. Hunn JD. "Results from ORNL Characterization of Nominal 350 μm NUCO Kernels from the BWXT 59344 Batch." Document# ORNL/CF-05/02. Feb 2005.
5. BWXT Nuclear Products Division report. G73 Industrial Fuel Fabrication and Development: Lot G73D-20-69302. Mar 2005.

ADVANCED GAS REACTOR PROGRAM
OAK RIDGE NATIONAL LABORATORY

ORNL DOCUMENT CLEARANCE / REGISTRATION FORM

PERSON PREPARING FORM: J. D. Hunn	PHONE NO.: 574-2480	DATE SUBMITTED: August 02, 2005
DOCUMENT NO.: ORNL/TM-2005/517	SPONSOR: DOE-NE / Dr. Madeline Feltus	
TITLE: Results from ORNL Characterization of Nominal 350 μ m LEUCO Kemels from the BWXT Q73D-20-69302 Composite		
AUTHOR(s): A. K. Kercher and J. D. Hunn		
SIGNATURES:		
AUTHOR:		
 Name: J. D. Hunn		<u>8-9-05</u> Date
TECHNICAL REVIEWER:		
 Name: O. M. Stanfield		<u>9 August, 2005</u> Date
APPROVER:		
 Name: G. L. Bell		<u>August 9, 2005</u> Date